Pergamon

Acta mater. Vol. 46, No. 15, pp. 5579–5591, 1998

Printed in Great Britain
PII: S1359-6454(98)00167-0
1359-6454/98 $19.00 + 0.00

STRESS-INDUCED MARTENSITIC TRANSFORMATION OF A NiTi ALLOY IN ISOTHERMAL SHEAR, TENSION AND COMPRESSION

L. ORGÉAS† and D. FAVIER

Laboratoire Sols, Solides, Structures, UMR CNRS 5521, Université Joseph Fourier Grenoble I, Institut National Polytechnique de Grenoble, BP 53X, 38041 Grenoble Cedex 09, France

(Received 22 September 1997; accepted 20 April 1998)

Abstract—The thermomechanical behaviour of stress-induced martensitic transformation in an equiatomic NiTi alloy was investigated with respect to different deformation modes including uniaxial tension, compression and shear of plate specimens at different temperatures above the M_s temperature. Results showed that loading conditions have significant influences on the deformation behaviour of the alloy. In particular, deformation behaviour was observed to be asymmetric in tension and in compression. The physical origins of such an asymmetry are explored. Comparison among the results obtained from the tension, compression and shear tests disproves the use of classical Von Mises equivalent in the modelling of the three-dimensional behaviour of martensitic transformation in this alloy. Based on this analysis, another criterion for yielding, which involves the third stress invariant, is therefore suggested. © *1998 Acta Metallurgica Inc. Published by Elsevier Science Ltd. All rights reserved.*

Résumé—Le comportement thermomécanique de la transformation martensitique induite sous contrainte dans un alliage NiTi équiatomique a été étudié à différentes températures supérieures à M_s et sous différents chemins de sollicitation, à savoir la traction, la compression et le cisaillement. Les résultats ont montré que les conditions de chargement ont une influence significative sur la déformation du matériau. En particulier, les comportements en traction et compression ne sont pas symétriques: les raisons physiques d'une telle dissymétrie sont discutées. La comparaison des résultats de traction, de compression et de cisaillement montre l'incapacité des équivalents classiques de type Von Mises à modéliser le comportement tri-dimensionnel de la transformation martensitique du présent matériau. A partir des résultats précédents, un autre critère macroscopique faisant intervenir le troisième invariant du tenseur des contraintes est alors proposé. © *1998 Acta Metallurgica Inc. Published by Elsevier Science Ltd. All rights reserved.*

1. INTRODUCTION

Shape memory alloys (SMAs) have attracted extensive interest in scientific research in the past several decades, owing to their novel properties. Among these properties, superelasticity, shape memory effect and two-way memory effect are known to be closely related to thermoelastic martensitic transformation, a first-order displacive thermoelastic solid–solid phase transformation [1]. Owing to a vast variety of experimental evidence, significant progress has been made in the characterization and the understanding of these behaviours. Nevertheless, there still remains a lack of knowledge.

As a matter of fact, most experimental studies of the thermomechanical behaviour of SMAs to date have been conducted in uniaxial tension, with few being carried out in other homogeneous stress state conditions. It has been demonstrated in the literature with these studies that the thermomechanical behaviour of a specimen is sensitive to the deformation mode. Significant differences have been observed between tension and compression for both NiTi [2, 3] and CuZnAl [4] alloys. Furthermore, Manach and Favier [5] have demonstrated that the Von Mises assumptions, that are usually adopted in establishing tensorial constitutive equations, are not always valid in simple shear tests for NiTi alloys. This implies that conclusions derived from tensile deformation tests cannot be directly translated to other deformation modes and that independent experimental investigations of deformation modes other than tension are needed for a full characterization of the thermomechanical behaviour of NiTi. To date, however, no directly comparable studies have been carried out to investigate the effects of deformation modes, such as tension, compression and shear, using the same SMA to describe the behaviour of stress-induced martensitic transformations. Such experimental evidence is essential both for the understanding of the phenomena of shape memory effects and for the establishment of three-dimensional constitutive equations [6–10]. For this reason, this study was carried out aiming at investigating the effects of deformation modes, including

†To whom all correspondence should be addressed.

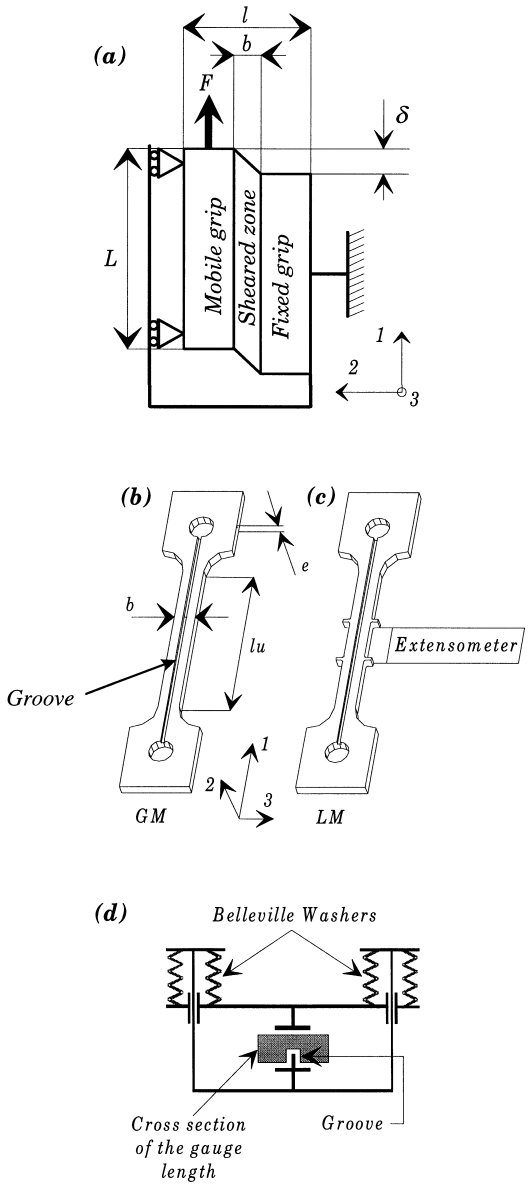

Fig. 1. Experimental facilities: (a) oversimplified scheme of simple shear test; (b, c) tension–compression samples without (b) and with (c) special shapes to fix an extensometer; (d) oversimplified scheme of the anti-buckling device.

tension, compression and simple shear, on the behaviour of the stress-induced martensitic transformation of an industrial equiatomic NiTi alloy. The experimental results of this study are presented in this paper together with discussions on three-dimensional modelling of the phenomena.

2. EXPERIMENTAL PROCEDURE

2.1. Material

The material used was a commercial polycrystalline equiatomic NiTi alloy supplied by Mémométal Industries (France). It was received in two sheets of 3.2 and 1.3 mm in thickness, respectively. The 3.2 mm sheet was used for tension–compression tests and the 1.3 mm sheet was used for shear tests. The as-received sheets were homogenized at 1173 K for 3.6 ks, followed by a cold rolling of ≈18% thickness reduction to 2.7 and 1.05 mm for the two sheets, respectively. After the cold working, the sheets were annealed at 703 K for 1.8 ks. After such treatments, the material showed a two-step $A \rightarrow R \rightarrow M$ transformation on cooling and a one-step $M \rightarrow A$ transformation on heating, as determined by differential scanning calorimetry. The critical temperatures of the transformations were measured to be $R_s \approx 321$ K, $R_f \approx 308$ K, $M_s \approx 283$ K, $M_f \approx 226$ K, $A_s \approx 301$ K and $A_f \approx 328$ K.

2.2. Specimens

Specimens for all tests were fabricated by spark-cutting from the sheets after the treatment described above. Shear specimens were rectangular in shape of $30 \times 18 \times 1.05$ mm^3, with a shear gauge section of $30 \times 3 \times 1.05$ mm^3 and a shear direction along the length of the specimens. This gave a length-to-width ratio of $L/b = 10$ for the shear gauge section. Under this condition, the shear stress τ is considered homogeneous inside the gauge zone [11, 12]. Specimens for tension–compression tests were bone-shaped sheet specimens as shown in Fig. 1(b) and (c). The deformation gauge section of the specimens was 40 mm in length (l_u), 5.6 mm in width (b) and 2.7 mm in thickness (e). To enable compressive loading on such specimens, a specially designed anti-buckling gripping system was designed, as schematically shown in Fig. 1(d). The use of the Belleville washers ensured that this system did not constrain the expansion of the cross-section of a specimen during compression. A thin groove with a cross-section of 1.2×0.8 mm^2 was machined out on one side of the specimens to fit with the anti-buckling system. The performance of this anti-buckling system has been reported earlier [13].

2.3. Mechanical testing

Three different deformation modes were employed for mechanical testing, tension, compression and simple shear. All the three tests were performed on an Adamel-MTS universal mechanical testing machine with different gripping and deformation mechanisms suitable for the three deformation modes. The shear testing device and a shear specimen after a certain amount of shear deformation are schematically shown in Fig. 1(a) [5]. The device consisted a stationary grip (right) and a mobile grip (left), which moved in the vertical direction. A loadcell of 20 kN capacity was used for all three tests. Tests were carried out at different temperatures between 243 and 373 K. The testing temperature was controlled with an accuracy of ± 1 K using a silicon oil bath and an ultracryothermostat Huber HS900. To minimize the thermal effect associated with the release and the absorption of the

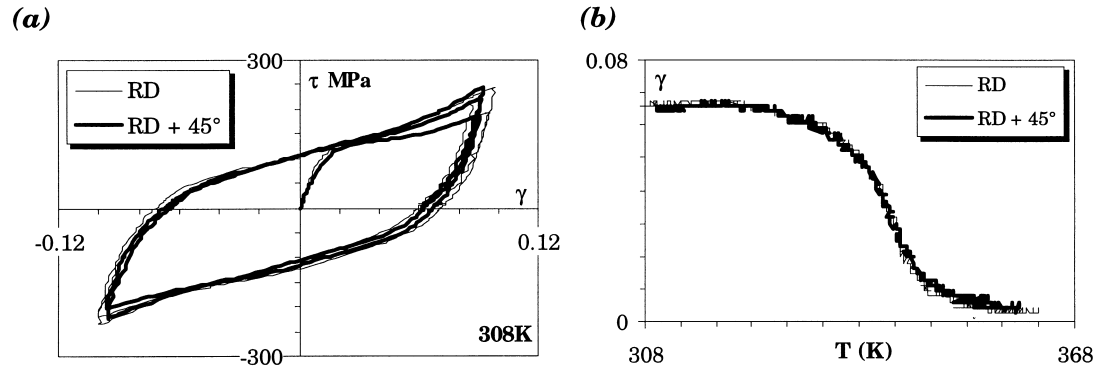

Fig. 2. Isotropy of the sheets: (a) isothermal shear stress–strain curves (T = 308 K) for two specimens: rolling direction (RD) and 45° from RD (RD + 45); (b) shape recovery of these two specimens.

latent heat of the martensitic transformation on the mechanical behaviour of a specimen [14], all tests were performed with low strain rates, i.e. $d\varepsilon/dt = 10^{-3}$/s for tension and compression testing and $d\gamma/dt = 1.75 \times 10^{-3}$/s for shear testing.

2.4. Stress and strain measurements

For tension–compression tests using specimens in the geometry shown in Fig. 1(b), the measurement of the total length variation of the sample, i.e. the global strain (GM), was measured as the axial strain of the specimens. These tests were carried out mainly to study transformation stresses. For tension–compression tests using specimens shown in Fig. 1(c), local axial strain (LM) was measured with an extensometer mounted on the specimen in the oil bath. The gauge length of the extensometer was 10 mm. In this work, engineering stress and engineering strain are used to plot tension and compression results, unless otherwise specified. For the shear tests, the extensometer was mounted on the two grips in the oil bath; thus a local measurement (LM) of shear strain can be estimated as $\gamma = \delta/b$, where δ is the local measurement of the relative vertical motion of the mobile grip with respect to the stationary grip, and b the width of the sheared zone [see Fig. 1(a)]. The shear stress t is estimated as $F/(L \times e)$, where F is the applied force, L the length of the specimen and e its thickness [see Fig. 1(a)].

2.5. Isotropy of the material

To identify isotropic conditions of the sheets after cold rolling, several shear specimens were cut from the 1.05 mm sheet at different orientations relative to the rolling direction [5]. Shear stress–strain curves of two samples, one in the rolling direction (RD) and the other in a direction 45° from the rolling direction (RD + 45°), are shown in Fig. 2(a). These two orientations are expected to give the greatest difference for any anisotropy that might be caused by the cold rolling [5]. The two samples were deformed at T = 308 K for several cycles between $\gamma = \pm 9\%$. The testing temperature was reached by cooling the samples from 373 K. The two specimens exhibited identical deformation behaviour, both during initial loading, which was a stress-induced martensitic transformation process, and during subsequent cycling, which was a martensite reorientation process. The cyclic deformation was terminated at $\gamma \approx 7\%$ at τ = 0 MPa for both samples. Figure 2(b) shows the shape recovery of the two samples upon heating after the deformation. Please note that the two samples exhibited similar shape memory effect. These observations suggest that the sheet material had a planar isotropy (revolution orthotropy) after the above-mentioned procedure of treatment. Moreover, microhardness tests were also performed in the martensitic state with a 0.5 kg load at different locations on the top and the lateral surfaces of the sheets, showing a constant value of $300HV_{0.5}\pm2\%$. These measurements suggest that the sheet material had a full isotropy.

2.6. Influence of the thickness

Compression tests were performed using the 2.7 mm sheet to minimize the problem of buckling. To establish the comparability between compression–tension tests and shear tests, which utilized the 1.05 mm sheet, identical tensile tests were performed on the two sheets. Figure 3 shows the deformation behaviour and the shape memory recovery of two specimens of 2.7 and 1.05 mm thickness, respectively. The specimens were deformed in tension at 308 K via a stress-induced martensitic transformation and then heated to above A_f temperature under no loading for shape recovery. The deformation temperature was reached by cooling the specimens from 373 K. It is seen that the two specimens exhibited practically identical deformation behaviour. The shape memory recovery of the 2.7 mm sheet specimen seemed to start at a slightly higher temperature and to occur over a slightly wider temperature range as compared to the 1.05 mm sheet specimen. This is attributed to a thermal hysteretic effect to the heating of the

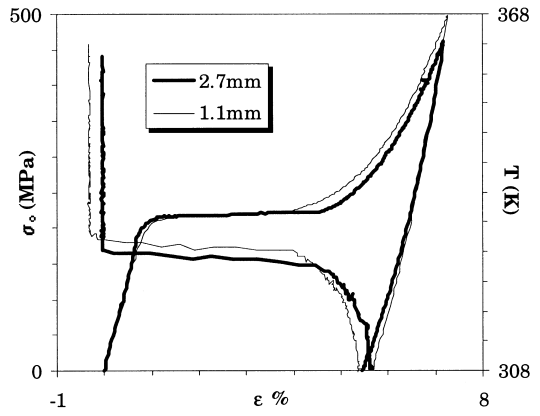

Fig. 3. Influence of the sheet thickness during stress-induced martensitic transformation at $M_s<T<A_f$ and during shape memory effect.

thicker specimen relative to the thinner specimen. In conclusion, the two sheet materials are considered as having the same thermomechanical behaviour.

3. ISOTHERMAL TESTS

3.1. Asymmetric deformation behaviour between tension and compression

Isothermal tension–compression tests were carried out at above A_f to investigate the critical stresses required to induce martensite in tension and in compression. Accurate strain measurement was not essential and the global measurement *GM* of deformation was recorded. Three tension–compression stress–strain loops are shown in Fig. 4(a) of the same sample tested at 333, 338 and 343 K sequentially. The sample exhibited superelasticity at all three temperatures. The critical stresses required to induce the martensitic transformation in both tension and compression increased with increasing testing temperature. The superelastic behaviour, however, showed a significant difference between the two deformation directions. The critical stress and stress hysteresis of the superelastic behaviour were larger in compression than in tension.

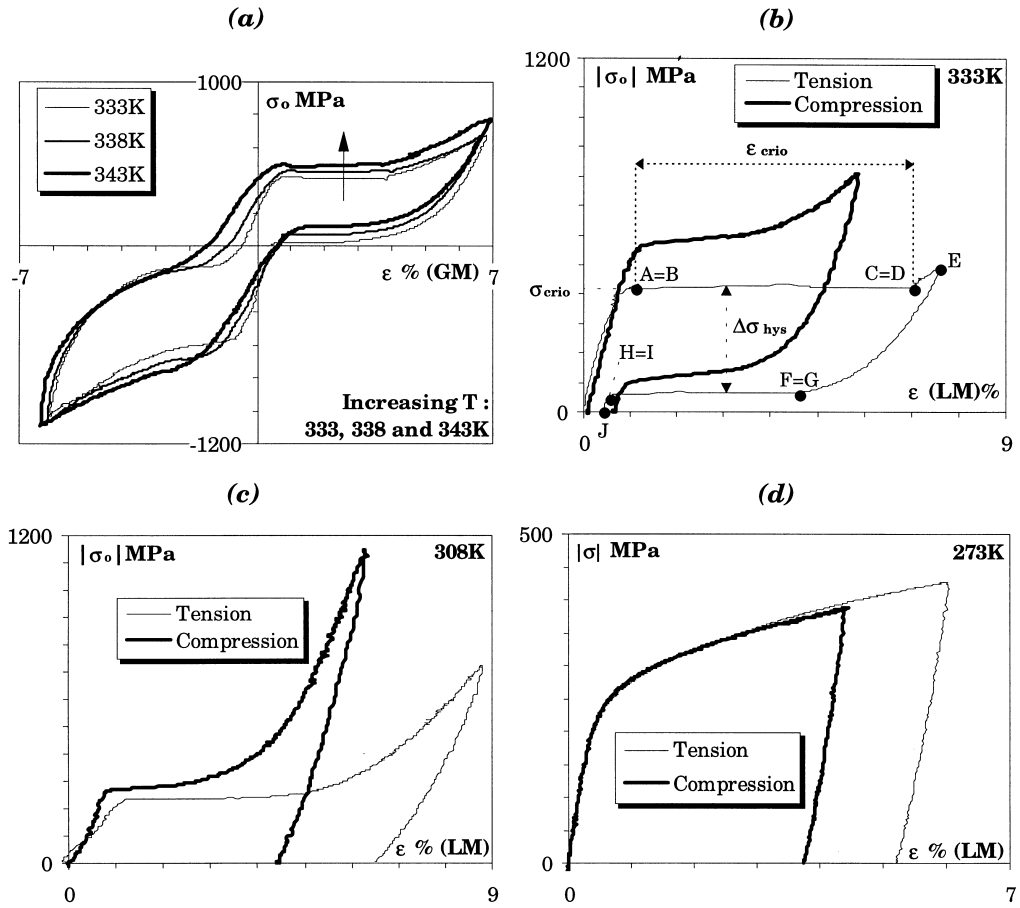

Fig. 4. Isothermal tension and compression experiments: tension–compression loops at T = 333, 338, 343 K with global strain measurement (a); tension and compression tests performed on two virgin austenitic samples at $T>A_f$ (b) and at $M_s<T<A_f$ (c) using local strain measurement; tension and compression tests performed on two virgin martensitic samples at $M_f<T<A_s$ using local strain measurement and true stress values (d).

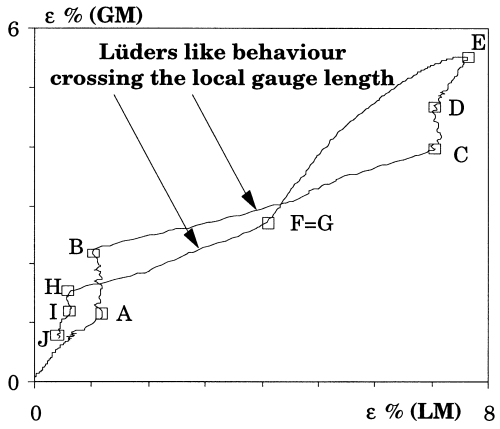

Fig. 5. Lüders-like behaviour in tension: global strain measurement vs local strain measurement measured during the tensile test of Fig. 4(b).

3.2. Monotonic loading in tension and compression

Four samples were tested by monotonic loading in either tension or compression to eliminate any potential problems that might be associated with the direction of the initial loading and with cyclic loading. Two of the samples were tested at 333 K, which was 5 K above A_f, in tension and compression, respectively, and the other two were tested at 308 K, which was between M_s and A_f. All the four samples were deformed by stress-induced martensitic transformation. The stress–strain curves of the two pairs of samples are shown in Fig. 4(b) and (c), respectively. In these tests, local strain was measured. It is seen that at both temperatures, the specimens exhibited asymmetric deformation behaviour associated with the stress-induced martensitic transformation between tension and compression. The critical stress for stress-induced martensitic transformation, σ_{crio}, as conventionally defined in Fig. 4(b), was higher in compression than in tension. The strain associated with the transformation, ε_{crio}, also defined in Fig. 4(b), had an average value of $5.5 \pm 0.25\%$ in tension and $4.0 \pm 0.25\%$ in compression, giving a strain ratio of $\varepsilon_{criot}/\varepsilon_{crioc} = 1.375$.

The symmetry of the deformation behaviour between tension and compression was also tested for martensite. Two other samples were cooled in liquid nitrogen to be fully martensitic and then deformed at 273 K, 28 K below A_s, in tension and compression, respectively. Figure 4(d) shows the stress–strain curves of these two samples. In this figure true stresses and strains are presented, respectively, defined as $\sigma = \sigma_0(1 - \varepsilon)$ and $\varepsilon_l = \ln(1 + \Delta l/l_u)$, because the deformation was obviously homogeneous, as evidenced by the absence of Lüders-like behaviour. In this case, the deformation behaviour was identical in tension and compression.

3.3. Lüders-like deformation behaviour

It was noticed in the experiment that during the forward and reverse transformations in tension, a typical Lüders-like deformation behaviour occurred, as evident in Fig. 4(a) and (b). A Lüders-like deformation behaviour is characterized by a distinctive stress plateau on an engineering stress–strain curve. Figure 5 shows the measurement of the global strain (*GM*) as a function of the local strain (*LM*) for the tensile sample shown in Fig. 4(b) to illustrate the heterogeneous nature of the Lüders-like deformation behaviour. The corresponding points on the curves shown in Figs 5 and 4(b) are labelled identically. It is seen that in the initial stage of deformation between OA, the deformation was homogeneous, as indicated by the simultaneous increase of *LM* and *GM*. At the onset of the stress plateau at A [Fig. 4(b)], *LM* ceased increasing until B whilst *GM* continued to increase, indicating that a localized deformation occurred outside of the gauge section of the extensometer. In section BC, the increase of *LM* was more rapid relative to that of *GM*. This implies that the localized deformation band was propagating inside the gauge length of the extensometer. The localized deformation band exited the extensometer gauge length at C, as evidenced by the constant *LM* following. In section DE, the deformation resumed to be homogeneous again. During unloading, the specimen deformed homogeneously between EF, heterogeneously in FGHI and homogeneously again along IJ. Within the stages where Lüders-like deformation occurred, it is practically impossible to describe the true deformation state at a location by either *LM* or *GM* measurements. It needs to be pointed out that the Lüders-like deformation behaviour was only observed in tensile testing in this study. In compression and shear tests only homogeneous deformation was observed, as evident in Figs 4(a)–(c) and Fig. 6.

The Lüders-like behaviour is often observed in tension of NiTi alloys [14–18]. Its occurrence is affected by both intrinsic physical origins, like density and configuration of dislocations, grain size, precipitates, and extrinsic causes such as geometrical effects of specimen shapes and sizes [17]. Lüders-like behaviour imposes problems in the study of mechanical behaviour. When it occurs (portions AD and FI in Fig. 5), the actual stress–strain state inside the specimen is fully heterogeneous and unknown. The analysis of partial transformation is thus irrelevant, because the transformation is total in some regions of the sample and does not occur in other ones [18]. However, certain characteristic values defined in regions where the deformation is homogeneous remain meaningful, such as initial elastic domain, critical stress at the beginning of the transformation, and

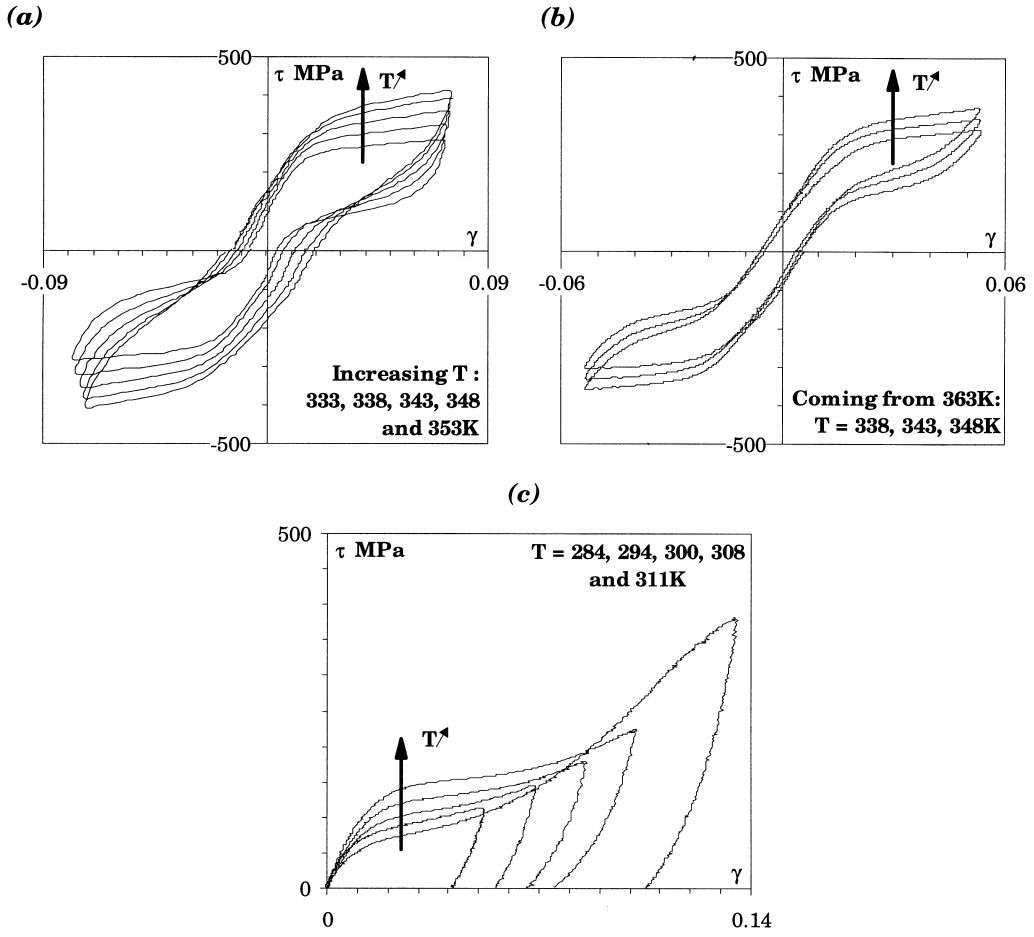

Fig. 6. Isothermal shear experiments at various testing temperatures T: (a) shear cyclic loading with an imposed strain magnitude $\Delta\gamma = \pm 7.5\%$ at $T > A_f$; (b) shear cyclic loading with an imposed strain magnitude $\Delta\gamma = \pm 5.5\%$ at $T > A_f$; (c) shear monotonic loading at $M_s < T < A_f$.

stress hysteresis of superelasticity when deformed to beyond the limit of transformation strain.

3.4. Shear tests

A shear specimen was deformed in superelasticity sequentially at five different temperatures of 333, 338, 343, 348 and 353 K with a shear strain magnitude of $\gamma \approx \pm 0.075$. The stress–strain curves of these tests are shown in Fig. 6(a). In these tests, the specimen was heated to 363 K after each test and then cooled to the next testing temperature. A second specimen was tested successively at 348, 343 and 338 K with a lower strain magnitude of $\gamma \approx \pm 0.055$. The measurements are shown in Fig. 6(b). It is seen that specimens exhibited a typical superelastic behaviour at all temperatures tested. A stress-induced $A \rightarrow R$ transformation was not observed and the superelastic deformation was associated with the stress-induced $A \rightarrow M$ transformation and the reverse $M \rightarrow A$ transformation. The critical stresses for both the forward and the reverse transformations increased with increasing testing temperature. A progressive deterioration of the superelastic behaviour with increasing temperature was also observed, as evidenced by the increase in the residual strain after unloading to $\tau = 0$ for the superelastic cycles. This is attributed to the increase in the contribution of plastic deformation with increasing temperature [19]. This effect was less pronounced for the deformation to lower shear strains [Fig. 6(b)].

Figure 6(c) shows the stress–strain curves of a sample tested at five different temperatures above M_s: 284, 294, 300, 308 and 313 K. After each test, the sample was heated to above A_f and cooled down to the next testing temperature. Therefore, the sample was in austenitic state prior to each test. During the loading, it is once again observed that the higher the testing temperature, the higher the stress to induce martensite. Upon unloading, the superelastic recovery is very small: stress levels reached during the loading were not high enough, and martensite reorientation processes occurred in this low temperature range [15].

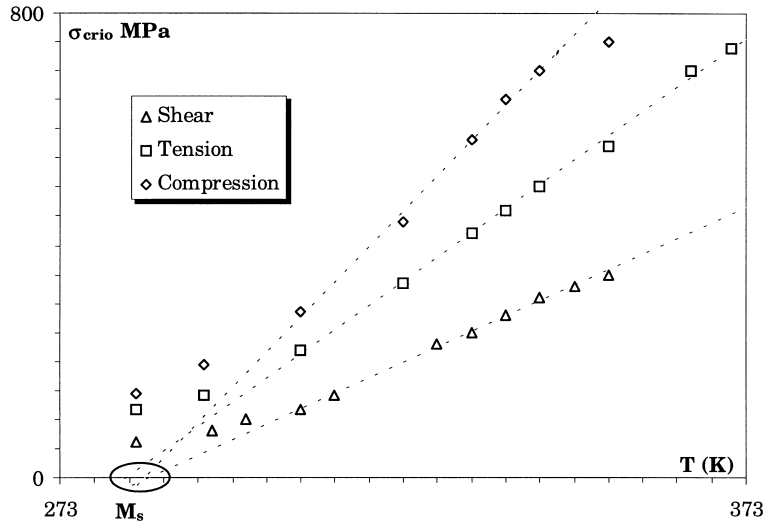

Fig. 7. Critical stresses as a function of both the temperature T and the loading path.

3.5. *Critical stresses for stress-induced martensitic transformation*

The critical stresses for stress-induced martensitic transformation in shear (τ_{crio}), tension (σ_{criot}) and compression (σ_{crioc}) as measured from the stress–strain curves, are plotted as functions of testing temperature in Fig. 7. In this figure three temperature ranges can be recognized. At temperatures below 308 K, the increase of the critical stresses with temperature was slow for all the three loading modes. At temperatures between 308 and 343 K, the critical stresses were linear functions of the testing temperature. Above 343 K, the temperature dependence of the critical stress in compression was no longer linear, suggesting that the influence of plastic deformation became more pronounced. For tension and shear the linearity of the temperature dependence of the critical stresses extended up to 370 and 353 K, respectively. The linear dependence of transformation stresses on temperature in the intermediate temperature range has been shown to obey a Clausius–Clapeyron relation [20]. In this work, $[d\tau_{crio}/dT]$ was measured to be 5.3 MPa/K in shear and $[d\sigma_{crio}/dT]$ to be 8.4 and 12 MPa/K in tension and compression, respectively. The slopes for shear and tension can be compared to those reported in the literature. The tension value agrees well with the data given by Tang *et al.* [21] for a wide number of NiTi alloys. Adler *et al.* [22] reported a slope of 3.45 MPa/K for shear and a slope of 10 MPa/K for tension for a NiTiCo alloy. Manach [23] obtained slopes of 5 and 7.5 MPa/K for shear and tension, respectively, for a NiTi alloy. In another work, Manach and Favier obtained slopes of 3.45 and 4.5 MPa/K for shear and tension, respectively, on a NiTi alloy submitted to a different prior thermomechanical treatment [5]. These measurements indicate that the slope is strongly influenced by the initial treatment conditions [19, 24–26].

Likewise, it is seen in Fig. 7 that the temperature dependence of the critical stress for stress-induced martensitic transformation was strongly influenced by the deformation mode. The ratio of the critical stress in tension to that in shear, $\sigma_{criot}/\tau_{crio}$, was found to be $\approx$1.7 at above 300 K, which agrees with a previous measurement of 1.75 at above A_f [5]. In both cases, the ratio is in good accordance with the Von Mises criterion ratio of $\sqrt{3}$. However, the ratio between the compression and tensile critical stresses, $\sigma_{crioc}/\sigma_{criot}$, and the ratio between the compression and shear critical stresses, $\sigma_{crioc}/\tau_{crio}$, took mean values of 1.33 and 2.26 for the same temperature range, respectively. According to the Von Mises criterion, these last ratios should be equal to 1 and $\sqrt{3}$, respectively. This disagreement requires another yield criterion to be established (Section 4.2).

3.6. *Stress hysteresis of superelasticity*

The stress hysteresis of superelasticity was measured on the stress–strain curves in shear ($\Delta\tau_{hys}$), tension ($\Delta\sigma_{hyst}$) and compression ($\Delta\sigma_{hysc}$), as illustrated in Fig. 4(b) for tensile deformation. Figures 8(a) and (b) show the effect of testing temperature on $\Delta\tau_{hys}$ for the shear tests shown in Figs 6(b) and (a), respectively. Comparison between Figs 8(a) and (b) shows that $\Delta\tau_{hys}$ was independent of testing temperature for superelastic loops of small strain amplitude ($\gamma = \pm 0.055$) and dependent of testing temperature for superelastic loops of large strain amplitude ($\gamma = \pm 0.075$). This is attributed to the involvement of plastic deformation in superelastic deformation with large strain amplitude. The two curves tested at 338 K are replotted together in Fig. 8(c) to illustrate the effect of strain amplitude on $\Delta\tau_{hys}$. It is seen that $\Delta\tau_{hys}$ increased with increasing strain amplitude. For $\gamma = \pm 0.075$,

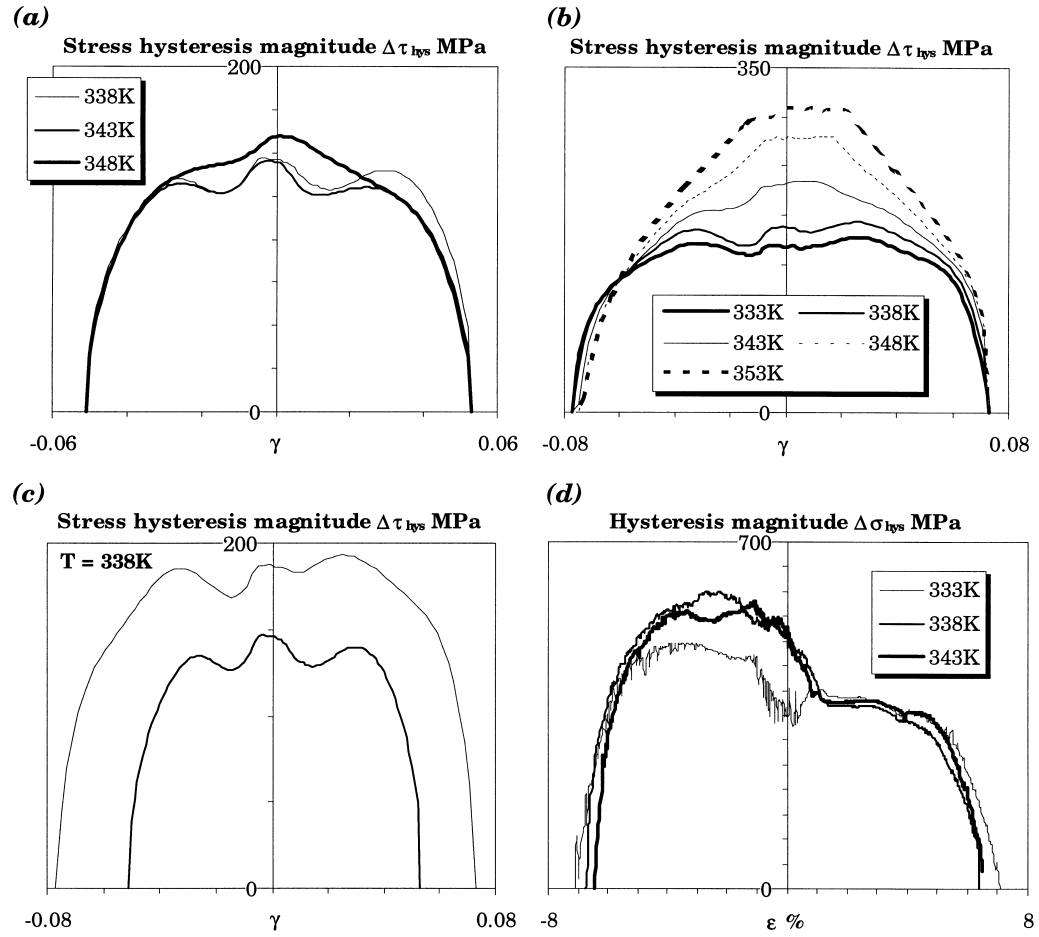

Fig. 8. Stress hysteresis magnitude as a function of: (a, b) the temperature in shear; (c) the imposed strain magnitude in shear; (d) the loading path in tension–compression.

$\Delta\tau_{hys} \approx 180$ MPa whereas for $\gamma = \pm 0.055$ it was ≈ 140 MPa [27]. Figure 8(d) shows the stress hysteresis of superelasticity in tension and compression, as measured from the stress–strain curves shown in Fig. 4(a). A significant asymmetry in $\Delta\sigma_{hyst}$ between tension and compression is clearly evident in the figure, with the hysteresis in compression, $\Delta\sigma_{hysc}$, being higher than that in tension, $\Delta\sigma_{hyst}$. It is also evident in the figure that whereas $\Delta\sigma_{hyst}$ was temperature independent at a value of 400 MPa, $\Delta\sigma_{hysc}$ was measured as 500 MPa at 333 K and 580 MPa at 338 and 343 K.

4. ANALYSIS

4.1. Tension–compression asymmetry

An asymmetric deformation behaviour of the stress-induced martensitic transformation was observed between tension and compression in this study. An asymmetric deformation behaviour may be caused either by intrinsic reasons of the transformation or external reasons related to experimental conditions as well as specimen texture. It has been established in Section 2 that the material was homogeneous and behaved isotropically. Therefore, internal stresses and texture induced by cold rolling could not be responsible for the observed asymmetry in deformation behaviour. A previous study [13] has demonstrated that the anti-buckling system, when correctly adjusted, does not induce any apparent asymmetry in deformation behaviour between tension and compression. Furthermore, Section 3 has proved that strength differential effect was observed since the first loading: it is not induced by mechanical cycling. It has also been established that martensite reorientation deformation proceeds symmetrically between tension and compression at low strain values [2, 28]. Based on these observations, it is concluded that the asymmetric deformation behaviour is an intrinsic property of the stress-induced martensitic transformation.

The phenomenon of asymmetric deformation behaviour between tension and compression has been observed in a number of alloy systems [29]. This phenomenon is usually referred to as the strength differential effect (SDE). For SMAs, it has been observed in NiTi polycrystalline during martensite reorientation to high strain values [2, 28] and

in CuAlZn polycrystalline samples during stress-induced martensitic transformation [4]. Several mechanisms have been proposed to explain SDE.

4.1.1. Role of hydrostatic pressure. A hydrostatic pressure may influence a phase transformation if it involves a volume change. This concept has been adopted to explain the SDE observed in quenched and tempered steels [29]. In this case, the yield strength is found to be higher in compression than in tension, because of a positive volume change during plastic deformation. In the case of NiTi alloys, the relative volume change $\Delta V/V$ associated with the martensitic transformation is very small ($<0.1\%$) and is negative [30]. A negative volume change is expected to cause an increase of M_s with increasing hydrostatic pressure. This has actually been observed in a NiTi alloy by Kakeshita *et al.* [31]. The p-dependence of M_s was measured as ≈ 0.01 K/MPa. The positive p-dependence of M_s due to the negative volume change implies that the critical stress for the martensitic transformation is higher in tension than in compression. Therefore, the effect of hydrostatic pressure, or the volume change associated with the transformation cannot be held responsible for the observed asymmetry in deformation behaviour between tension and compression.

In contrast, the magnitude of asymmetry of the deformation behaviour is expected to have been reduced by this effect. The reduction in the critical stress for transformation in compression relative to that in tension can be estimated as follows, for the specimens tested at 333 K [Fig. 4(b)] for example. The critical stresses for stress-induced martensitic transformation were 420 MPa for the specimen tested in tension and 570 MPa for the specimen tested in compression, giving a stress difference of $\sigma_{cri} = 150$ MPa. The hydrostatic components of the stresses, $p = \mathrm{tr}[\boldsymbol{\sigma}]/3$, are estimated to be 140 and -190 MPa for the two specimens, respectively. With a p-dependence coefficient of 0.01 K/MPa, this hydrostatic pressure difference of $p = 330$ MPa causes an M_s in compression to be 3.3 K higher than that in tension. Applying the Clausius–Clapeyron relation with an average value of $\mathrm{d}\sigma_{cri}/\mathrm{d}T = (8.4 + 12)/2 = 10.2$ MPa/K, the transformation stress in compression is thus estimated to be 33.6 MPa higher than that in tension due to the effect of the volume change. Taking this effect into account, the magnitude of asymmetry as measured as the critical stress difference between tension and compression is thus $\sigma_{cri} = 150 + 33.6 = 183.6$ MPa at 333 K.

4.1.2. Microstructural aspects of martensitic transformation. A second possible contribution to the deformation asymmetry is based on microstructural considerations of the martensitic transformations in SMAs. For single crystal specimens, the dependence of the macroscopic tensile transformation stresses and strains on orientation has been well studied experimentally [32–34]. Some experiments have been carried out using CuAlNi single crystals to study the symmetry of the deformation behaviour in tension and compression for given crystallographic orientations [35]. Based on these experiments, three types of models have been proposed to describe the orientation dependence as well as the tension–compression asymmetry of the stress-induced martensitic transformation strain in SMA single crystals.

4.1.2.1. The PTMC-based Models

A first type of models are based on the phenomenological theory of martensite crystallography (PTMC) [36, 37]. In the PTMC, the total strain of an internally twinned or faulted martensite from the austenite, $\mathbf{P}_{tot}$, is expressed as the product of a Bain strain $\mathbf{B}$ between the parent and martensite phases, the lattice invariant shear (LIS) $\mathbf{P}$, and a rigid body rotation $\mathbf{R}$, i.e. $\mathbf{P}_{tot} = \mathbf{RPB}$. In a NiTi single crystal, the LIS results from the formation of twin-related martensite variant pairs, which are referred to as correspondence variant pairs (CVPs) [38]. Using a PTMC-based model, Buchheit *et al.* [38] concluded that the asymmetric tension–compression behaviour of SMA single crystals was an intrinsic property of the thermoelastic martensitic transformation. According to the authors, the CVPs induced in tension were different from the ones induced in compression, especially for NiTi single crystals. Their numerical calculations showed a good agreement with tensile experimental results for a long-aged NiTi single crystal [33] which contained precipitates. However, transformation strains predicted by the PTMC models are often smaller than those measured in experiments, especially for single crystals which do not contain many precipitates [33].

The application of the PTMC models to polycrystalline materials is not straightforward. In that respect, several micro–macro theories based on the PTMC have been proposed in order to predict the mechanical behaviour of polycrystalline SMAs [39–41]. Ono and Shimanuki [39] used the PTMC approach to determine the modified Taylor factors for the martensitic transformations in a number of non-textured polycrystalline SMAs such as CuZnAl, CuAlNi and NiTi. They concluded that the theoretical predictions conformed to the Von Mises criterion. Their predictions are in disagreement with our experimental results on NiTi and those of Vacher [4] on CuZnAl. Patoor *et al.* [40] used both a PTMC-based model and a self-consistent scheme to analyse the mechanical behaviour of isotropic CuZnAl polycrystalline samples and revealed a tension–compression asymmetry. They showed that the very small volume variation associated with the martensitic transformation was not responsible for the SDE. They also found that both the critical stress for transformation and the magnitude of stress hysteresis were higher in compression

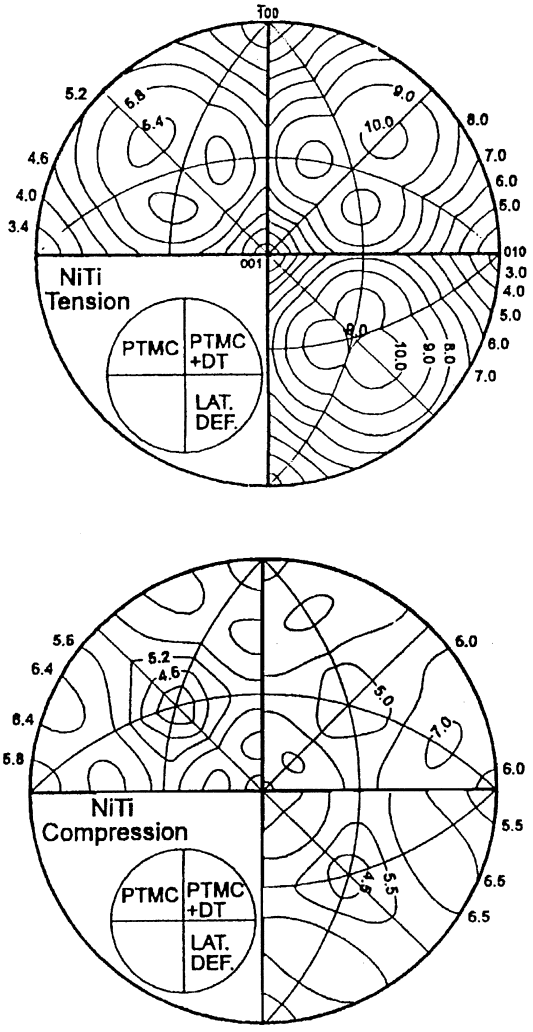

Fig. 9. Contour plots within [001] stereographic projections illustrating and comparing the tensile (circle 1) and the compressive (circle 2) transformation strain results from the PTMC model, the PTMC + DT model and the lattice deformation model—according to Buchheit and Wert [45].

than in tension, whereas it was the opposite for transformation strain. They attributed the SDE to two contributions, the low symmetry of the martensite structure and to the fact that the domain of well-oriented positions in each single crystal depends on the local loading condition. Their numerical results showed qualitative agreement with the experimental results of Vacher [4] for polycrystalline CuZnAl. However, when the same micro–macro model is applied to an isotropic polycrystalline NiTi, their calculation predicts that the critical stress for transformation is higher in tension than in compression [42, 43], being in total disagreement with the present results. The explanation proposed by Patoor *et al.* to the tension–compression asymmetry is thus inappropriate for NiTi alloys.

4.1.2.2. The Lattice Deformation Model

Using a lattice deformation model Saburi and Nenno [44] calculated the tensile martensitic transformation strains of NiTi single crystal samples. Such a model predicts the transformation strain considering direct transformation of an austenite single crystal to a single correspondence variant (SCV) of martensite. Therefore, the total distortion matrix $\mathbf{P}_{tot}$ is only determined by the Bain strain matrix **B**. In comparison, the transformation strain predicted by the lattice deformation model is generally larger than that predicted by PTMC-based models [45], as illustrated in Fig. 9. Transformation strains measured in experiments are often in better agreement with the lattice deformation model than with PTMC-based models, even for initially twinned or faulted martensites [33, 45]. Plietsch and Ehrlich tried to estimate with a similar micro model the ratio of the transformation strain in tension to that in compression, $\varepsilon_t/\varepsilon_c$, in an isotropic polycrystalline NiTi by simply averaging the values of $\varepsilon_t/\varepsilon_c$ for a large range of crystallographic orientations [3]. Their estimation, $\varepsilon_t/\varepsilon_c = 1.46$, agrees reasonably well with our experimental measurement ($\varepsilon_{criot}/\varepsilon_{crioc} = 1.375$). However, no quantitative conclusion can be drawn for two reasons. Firstly, the lattice deformation model does not reproduce all the mechanisms arising during the transformation of a SMA single crystal, i.e. the existence of a habit plane. Secondly, the basis to estimate the strain ratio of a polycrystalline matrix as the average for all crystallographic orientations is doubtful.

4.1.2.3. The PTMC + DT Model

In an analysis Buchheit and Wert [45] showed that the PTMC-based models did not concur with the experiments performed by Miyazaki *et al.* [33] on a NiTi single crystal. For the single crystal sample, Miyazaki *et al.* [33] observed that detwinning of CVPs to SCVs occurred during loading. To account for this observation, Buchheit and Wert included in their PTMC-based model the detwinning of CVPs to SCVs during loading and showed that transformation strains calculated from the lattice deformation model and from the PTMC + detwinning (PTMC + DT) model are almost equal, as illustrated in Fig. 9 [45]. However, they also reported that crystallographic mechanisms of transformation adopted by the two models are not equivalent: the lattice deformation model considers an austenite → SCV transformation whereas the PTMC + DT model involves a more realistic austenite → CVP → SCV transformation, compared to experimental observations [33, 46]. The predictions of the PTMC + DT model are in good agreement with the tensile behaviour of the solution treated NiTi single crystal of Miyazaki *et al.* [33], as well as with other SMA systems. The numerical analysis of Buchheit and Wert showed that the ten-

sile detwinning strain in tension ranges from 0 to 3.77%, depending on the tensile axis orientation with respect to the crystal orientation, whereas that in compression ranges from 0.57 to 0.68%. The overall transformation strain (PTMC + DT strains) in tension, $\varepsilon_{\mathrm{trt}}$, ranges from 7 to 10.31% and that in compression, $\varepsilon_{\mathrm{trc}}$, is between 5 and 7.11%, as illustrated by the stereographic representations shown in Fig. 9 [45]. Based on the concept of energy conservation, Buchheit and Wert expressed the work of transformation as

$$W_{\mathrm{meca}} = \gamma_{\mathrm{tr}}^{\mathrm{cri}} \cdot \tau_{\mathrm{tr}}^{\mathrm{cri}} = \varepsilon_{[hkl]}^{\mathrm{tension}} \cdot \sigma_{[hkl]}^{\mathrm{tension}} = \varepsilon_{[hkl]}^{\mathrm{compression}} \cdot \sigma_{[hkl]}^{\mathrm{compression}} \quad \forall [hkl] \qquad (1)$$

where $\tau_{\mathrm{tr}}^{\mathrm{cri}}$, $\sigma_{[hkl]}^{\mathrm{tension}}$ and $\sigma_{[hkl]}^{\mathrm{compression}}$ are the critical stresses for martensitic transformation in shear, tension and compression, and $\gamma_{\mathrm{tr}}^{\mathrm{cri}}$, $\varepsilon_{[hkl]}^{\mathrm{tension}}$ and $\varepsilon_{[hkl]}^{\mathrm{compression}}$ are the strain associated with the transformation in shear, tension and compression in the [*hkl*] crystal orientation, respectively. According to this equation, the critical stresses for transformation in compression are greater than that in tension for most crystallographic orientations, due to the higher transformation strains in tension than in compression.

Combined with a self consistent micro–macro approach similar to that adopted by Patoor *et al.*, the PTMC + DT model is expected to give a better description of the mechanical behaviour of polycrystalline NiTi. It is believed that the tension–compression asymmetry of the stress-induced martensitic transformation is mainly due to the detwinning strain contribution to the overall transformation strain. This detwinning strain is larger in tension than in compression, resulting in the transformation stress being higher in compression than in tension.

4.2. Mechanical modelling

According to the above discussion, the influence of hydrostatic pressure p on the mechanical behaviour has to be excluded. Hence, all the characteristic values such as transformation stress and strain are independent of the first stress invariant $I_\sigma = \mathrm{tr}(\boldsymbol{\sigma})$. This assumption is commonly adopted for metallic materials. Yield surfaces that can be used to model the critical stress as a function of the loading path can therefore be plotted in the deviatoric stress plane, instead of being expressed in the principal stress space. In such a plane, yield surfaces are functions of both the deviatoric stress tensor intensity Q_σ and phase φ_σ, as defined as

$$Q_\sigma = \sqrt{\mathrm{tr}[\bar{\boldsymbol{\sigma}} \cdot \bar{\boldsymbol{\sigma}}]}$$

and

$$\cos[3\varphi_{\bar{\sigma}}] = \sqrt{6}\,\mathrm{tr}[\bar{\boldsymbol{\sigma}} \cdot \bar{\boldsymbol{\sigma}} \cdot \bar{\boldsymbol{\sigma}}]/Q_\sigma^3 \qquad (2)$$

with

$$\bar{\boldsymbol{\sigma}} = \boldsymbol{\sigma} - \frac{1}{3} I_\sigma \mathbf{I} \quad \text{and} \quad \mathbf{I} = \text{unit tensor.} \qquad (3)$$

According to the present experimental results, no simple classical yield form is suitable to model the martensitic transformation in the NiTi alloy used in this study. For example, the frequently used Von Mises yield criterion cannot describe the tension–compression asymmetry, because it is independent of φ_σ. To reach such a goal, yield forms have to be functions of both Q_σ and φ_σ. Many appropriate yield surfaces have been proposed in such a way [40, 47, 48]. In the present work, the used yield criterion has been suggested by Stutz [49] and is expressed by the following relation:

$$Q_{\sigma_{\mathrm{cri}}} = Q_{\sigma_{\mathrm{crio}}}/[1 + \gamma_0 \cdot \cos(3 \cdot \varphi_\sigma)]^{n_0} \qquad (4)$$

which involves three parameters, $Q_{\sigma_{\mathrm{crio}}}$, γ_0 and n_0. Based on experimental data, these three parameters were determined by solving the system (4). The system is obtained by writing that during shear (first equation), tension (second equation) and compression (third equation), the phases of the deviatoric stress tensor φ_σ are equal to $\pi/6$, 0 and π, respectively

$$\sqrt{2}\tau_{\mathrm{cri}} = Q_{\sigma_{\mathrm{crio}}};$$

$$\frac{\sqrt{3}}{2}\sigma_{\mathrm{crit}} = \frac{Q_{\sigma_{\mathrm{crio}}}}{(1+\gamma_0)^{n_0}}\frac{\sqrt{3}}{2};$$

$$\sigma_{\mathrm{cric}} = \frac{Q_{\sigma_{\mathrm{crio}}}}{(1-\gamma_0)^{n_0}}. \qquad (5)$$

The curves plotted in Fig. 10 illustrate the evolution of $Q_{\sigma_{\mathrm{cri}}}$ with T and the loading path in the deviatoric stress plane for $T > M_{\mathrm{s}}$. Parameters n_0 and γ_0 have been fixed to constant values of 0.1 and 0.9, respectively. $Q_{\sigma_{\mathrm{crio}}}$ is linearly dependent on temperature, $[\mathrm{d}Q_{\sigma_{\mathrm{crio}}}/\mathrm{d}T]$ being equal to $\sqrt{2}[\mathrm{d}\tau_{\mathrm{cri}}/\mathrm{d}T] = 7.5\,\mathrm{MPa/K}$. Yield surfaces are in good agreement with experimental data (Fig. 10).

5. CONCLUSION

The isothermal mechanical behaviour of the stress-induced martensitic transformation in a NiTi alloy was investigated in this study. The experimental results demonstrated the importance of stress state on the deformation behaviour of the transformation. The deformation behaviour of the transformation was asymmetric between tension and compression. This asymmetry in mechanical behaviour is attributed to the low crystallographic symmetry of the martensite structure and the detwinning of the martensite. The experimental results also showed that no classical equivalent yield surface is suitable to model characteristic values such as transformation stress and strain as a function of the loading path. A yield surface depending on both the intensity and the phase of the deviatoric stress tensor was proposed, which

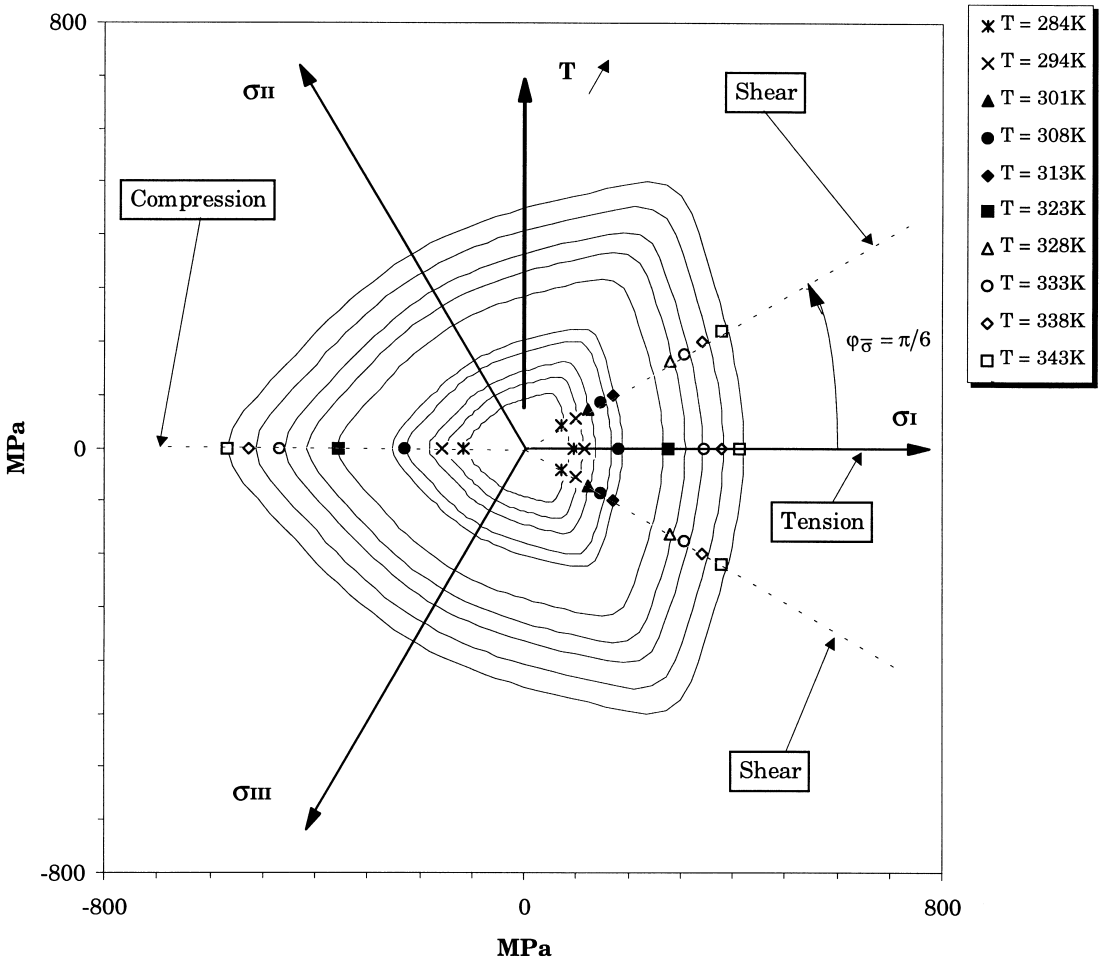

Fig. 10. Comparison of the experimental results (in tension, compression and shear) at different temperatures with the proposed yield criterion. This criterion is plotted using equation (3) with constant values of γ_0 (=0.9) and n_0 (=0.1) and a linear variation of $Q_{\sigma_{crio}}$ with T.

successfully modelled the experimental results of this study.

Acknowledgements—The authors wish to thank Yinong Liu for his valuable comments which contribute to the article being presented in the present form.

REFERENCES

1. Olson, G. B. and Cohen, M., *Scripta metall.*, 1975, **9**, 1247.
2. Wazilewski, R. J., *Metall. Trans.*, 1971, **2**, 2973.
3. Plietsch, R. and Ehrlich, K., *Acta mater.*, 1997, **45**, 2417.
4. Vacher, Ph.D. thesis, Université de Franche Comté, Besançon, France, 1991.
5. Manach, P. Y. and Favier, D., *Mater. Sci. Engng*, 1997, **A222**, 45.
6. Tanaka, K., Kobayashi, S. and Sato, Y., *Int. J. Plasticity*, 1986, **2**, 59.
7. Brinson, L. C. and Lammering, R., *Int. J. Solids Struct.*, 1993, **30**(23), 3261.
8. Raniecki, B. and Lexcellent, C., *Eur. J. Mech. A/Solids*, 1994, **13**, 21.
9. Favier, D., Habilitation thesis, INPG, Grenoble, France, 1988.
10. Favier, D., Guélin, P. and Pégon, P., *Mater. Sci. Forum*, 1990, **56-58**, 559.
11. Rauch, E. F. and G'Sell, C., *Mater. Sci. Engng*, 1989, **A111**, 71.
12. Wack, B. and Tourabi, A., *J. Mater. Sci.*, 1993, **28**, 71.
13. Orgéas, L. and Favier, D., *J. Physique IV*, 1995, **5**, 605.
14. McCormick, P. G., Miyazaki, S. and Liu Yinong, *Proc. Int. Conf. Martensitic Transformations*, Monterey, California, 1993, p. 999.
15. Liu Yinong, Favier, D. and Orgéas, L., *J. Physique IV*, 1995, **5**, 595.
16. Shaw, J. A. and Kyriakides, S., *J. Mech. Phys. Solids*, 1995, **43**(8), 1243.
17. Xiang, H., Liu Yinong and Bataillard, L., *Metall. Mater. Trans. A*, 1998, submitted.
18. Liu Yinong, Liu Yong and Van Humbeeck, J., *Scripta mater.*, 1998, to be published.
19. Liu Yinong, Ph.D. thesis, University of Western Australia, Perth, 1991.
20. Wollants, P., De Bonte, M. and Roos, J. R., *Z. Metallk.*, 1979, **2**(70), 113.
21. Tang, W., Cederström, J. and Sandström, R., *J. Physique IV*, 1991, **1**, 129.

22. Adler, P. H., Yu, W., Pelton, A. R., Zadno, R., Duerig, T. W. and Baresi, R., *Scripta metall.*, 1990, **24**, 943.
23. Manach, P. Y., Ph.D. thesis, INPG, Grenoble, France, 1993.
24. Lin, H. C. and Wu, S. K., *Acta metall.*, 1994, **42**(5), 1623.
25. Filip, P. and Mazanec, K., *Scripta metall.*, 1995, **32**(9), 1375.
26. Miyazaki, S., Ohmi, Y., Ostuka, K. and Suzuki, Y., *J. Physique IV*, 1982, **43**, 255.
27. Orgéas, L., Liu Yinong and Favier, D., *J. Physique IV*, 1998, **5,** 477.
28. Roumagnac, P., Ph.D. thesis, UTC, Compiègnes, France, 1993.
29. Spitzig, W. A., Sober, R. J. and Richmond, O., *Acta metall.*, 1975, **23**, 885.
30. Okamoto, K., Ichinose, S., Morii, K., Otsuka, K. and Shimizu, K., *Acta metall.*, 1986, **34**, 2065.
31. Kakeshita, T., Nakamichi, S., Tanaka, R., Endo, S. and Ono, F., *Mater. Trans. JIM*, 1992, **33**, 1.
32. Saburi, T., Yoshida, M. and Nenno, S., *Scripta metall.*, 1984, **18**, 363.
33. Miyazaki, S., Kimura, S., Otsuka, K. and Suzuki, Y., *Scripta metall.*, 1984, **18**, 883.
34. Horikawa, H., Ichinose, S., Morii, K., Miyazaki, S. and Otsuka, K., *Metall. Trans.*, 1988, **19A**, 915.
35. Sakamoto, H., Tanigawa, M., Otsuka, K. and Shimizu, K., *Proc. Int. Conf. Martensitic Transformations*, Cambridge, Massachusetts, 1979, p. 633.
36. Lieberman, D. S., Weschler, M. S. and Read, T. A., *J. appl. Phys.*, 1955, **26**, 473.
37. Bowles, J. S. and Mackenzie, J. K., *Acta metall.*, 1954, **2**, 129.
38. Buchheit, T. E., Kumpf, S. L. and Wert, J., *Acta metall.*, 1995, **11**, 4189.
39. Ono, N. and Shimanuki, H., *Scripta metall.*, 1990, **24**, 2269.
40. Patoor, E., El Amrani, M., Eberhardt, A. and Berveiller, M., *J. Physique IV*, 1994, **5**, 495.
41. Thuillier, S., Favier, D. and Canova, G., *J. Physique IV*, 1995, **5**, 587.
42. Personal communications with E. Patoor, unpublished results.
43. Personal communications with S. Thuillier, unpublished results.
44. Saburi, T. and Nenno, S., *Proc. Int. Conf. on Solid–Solid Phase Transformation*. The Metall. Soc. of AIME, 1981, p. 1455.
45. Buchheit, T. E. and Wert, J., *Metall. Trans.*, 1996, **27A**, 269.
46. Otsuka, K., Wayman, C. M., Nakai, K., Sakamoto, H. and Shimizu, K., *Acta metall.*, 1976, **24**, 207.
47. Krenk, S., *J. Engng Mech.*, 1996, 201.
48. Haythornthwaite, R. M., *Mech. Res. Commun.*, 1985, **12**(2), 87.
49. Stutz, P., Habilitation thesis, Université Joseph Fourier, Grenoble, France, 1979.